Effect of Direct Reduced Iron (DRI) on Dephosphorization of Molten Steel by Electric Arc Furnace Slag

JUNG HO HEO and JOO HYUN PARK

We investigated the effect of direct reduced iron (DRI) addition on dephosphorization of molten steel by electric arc furnace (EAF) slag at 1823 K (1550 °C). Various phenomena such as CO gas evolution and slagmaking by gangue oxides in DRI were experimentally observed at each reaction step. Thermodynamic behaviors of phosphorus, oxygen, and carbon were strongly dependent on DRI content. Basicity, which is the thermodynamic driving force of dephosphorization, decreased with the increasing DRI content because SiO_2 concentration in the slag was proportional to DRI addition. The excess free energy of P_2O_5 increased with the increasing SiO_2 content in slag. A higher DRI content made dephosphorization difficult by decreasing the basicity and stability of P_2O_5 in the slag. Therefore, when using DRI in EAF process, it is very important to control the basicity of slag.

https://doi.org/10.1007/s11663-018-1406-5

I. INTRODUCTION

THE use of direct reduced iron (DRI) as a substitute for premium scraps in electric arc furnace (EAF) steelmaking has increased in popularity because DRI does not have tramp elements, has a uniform density and shape, as well as higher yield and purity of carbon, affords convenience of charging, and has lower cost of raw materials.[1–7] Unfortunately, however, commercially available DRI contains a relatively high level of phosphorus, which adversely affects the properties of steels.[8,9] The increased use of DRI to produce high-quality steels in an EAF also increases the likelihood of phosphorus contamination of the steel. Thus, phosphorus should be fully controlled in the EAF process. However, because there are various types of oxides (*e.g.*, Fe_tO, SiO_2, Al_2O_3, CaO) as well as carbon present in DRI, a comprehensive understanding of the effect of DRI on slag formation behavior, and thus dephosphorization efficiency in the EAF process, is required.

The thermodynamic behavior of phosphorus in CaO-based slags containing various oxides and fluoride has been widely investigated. CaO-based slag is traditionally used in the steelmaking process because of its high refining ability and low cost.[10–22] Previous studies generally reported that phosphate capacity and the distribution ratio of phosphorus increased with the increasing CaO content, thereby increasing the stability of P_2O_5 by decreasing the activity coefficient of P_2O_5 in the slags. In other words, dephosphorization ability is strongly affected by CaO activity in CaO-based slags, and thus the phosphorus equilibria in CaO-saturated highly basic slags have been reported.[12,18,23,24]

Dephosphorization ability also depends on Fe_tO content in CaO-based slags because Fe_tO behaves as an acidic or basic oxide depending on the slag composition at a given oxygen potential. Lee and Fruehan[17] reported that the distribution ratio of phosphorus between carbon-saturated liquid iron and CaO-SiO_2-MgO-FeO slag increased with the increasing FeO content (3 to 10 mass pct) at 1823 K to 1853 K (1550 °C to 1580 °C) under an Ar atmosphere. In contrast, Hamano and Tsukihashi[16] reported that the distribution ratio of phosphorus between molten Fe-0.005 mass pct P and CaO-SiO_2-Fe_tO-MgO_{sat} (-B_2O_3) slags had a maximum point at approximate 45 mass pct Fe_tO content in a wide range of Fe_tO (FeO + Fe_2O_3 = 20 to 70 mass pct) at 1873 K (1600 °C) under a CO-CO_2 and Ar atmosphere. Similar results were also confirmed by the same research group[18]; the phosphate capacity of the CaO-SiO_2-Fe_tO-MgO_{sat} (-Al_2O_3, Na_2O) slags under a CO-CO_2 atmosphere for a range of Fe_tO contents (FeO + Fe_2O_3 = 40 to 70 mass pct) at 1823 K and 1873 K (1550 °C and 1600 °C) increased with the increasing FeO content up to 40 mass pct and decreased when FeO content exceeded 40 mass pct. They explained that the decrease in dephosphorization in high FeO content CaO-based slags was because of dilution of the CaO

JUNG HO HEO and JOO HYUN PARK are with the Department of Materials Engineering, Hanyang University, Ansan, 426-791, Korea. Contact e-mail: basicity@hanyang.ac.kr
Manuscript submitted May 29, 2018.
Article published online September 6, 2018.

content, which plays a major role in dephosphorization, *viz*., a decrease in the activity of CaO. An appropriate Fe_tO content in CaO-based slag is therefore important for dephosphorization.

Unfortunately, research on phosphorus behavior in an EAF process involving DRI is lacking because a high phosphorus content in DRI makes dephosphorization difficult. Fruehan and Manning[9] performed lab-based studies as well as EAF plant trials to examine the kinetic behavior of phosphorus in an EAF using commercial DRI. In their laboratory study, they evaluated dephosphorization kinetics by considering the apparent overall mass transfer coefficient and reported that a transient reduction in slag–metal interfacial tension during dephosphorization can lead to an increase in the reaction area due either to emulsification or enhancement of the mass transfer coefficient. Furthermore, they evaluated the mass transfer parameter in plant EAF trials and confirmed that the experimental data yielded very realistic and reproducible numbers for the phosphorous mass transfer parameter.

Lee *et al*.[25] confirmed a high content of P_2O_5 in molten slag (approx. 0.8 mass pct) using hot briquetted iron (HBI) up to 50 pct in plant trials at Sydney Steel Mill. Other EAF plant trials were performed in Casima, Venezuela, and these trials confirmed that a low content of phosphorus in molten steel (0.012 mass pct) was achievable even when using 85 pct HBI. Hassan *et al*.[26] reported that the increasing DRI content from 26 to 67 pct resulted in an increase in the phosphorus content in molten steel from 0.005 to 0.015 mass pct based on EAF trials performed in EZZ Flat Steel, Egypt.

Even though numerous studies have investigated the thermodynamics of phosphorus on a laboratory scale and several plant EAF trials have used DRI, our fundamental understanding of phosphorus behavior when using DRI is incomplete. In particular, the effects of various phenomena such as the carborthermic reaction between FeO and carbon in DRI, slagmaking by gangue melting in DRI, and oxygen transfer from slag produced by gangue melting to molten steel on the behavior of phosphorus during DRI melting still have to be clarified. Variation in slag composition is caused by the presence of gangue in DRI, which has a critical impact on dephosphorization efficiency. Therefore, in the present study, we investigated the effect of DRI on dephosphorization reaction between molten steel and EAF slag, and discussed the phosphorus partition behavior based on experimental results and thermodynamic investigation.

II. EXPERIMENTAL

Experiments were carried out using a high-frequency induction furnace, which is schematically illustrated in Figure 1. Steel (Fe-0.03Si-0.05Mn-0.03P-0.03S-0.1C, mass pct) and DRI (Fe-9FeO-5SiO_2-1CaO-0.02S-0.02P-1C, mass pct) were initially placed in a fused MgO (99.9 pct purity) crucible (outer diameter [OD]: 60 mm; inner diameter [ID]: 50 mm; height [HT]: 120 mm) with a graphite heater (OD: 80 mm; ID: 65 mm; HT: 120 mm) for induction heating. The crucible was surrounded by alumina insulation (OD: 104 mm; ID: 87 mm; HT: 180 mm). DRI was used as a steel (scrap in actual process) substitute by setting the total amounts of DRI and steel (*i.e*., DRI + steel) as 600 g. Mixing ratio of DRI in the DRI + steel samples was 0, 10, 20, or 30 mass pct.

A quartz reaction chamber (OD: 120 mm; ID: 114 mm; HT: 400 mm) with the experimental assembly was operated in a high-frequency induction furnace. The reaction chamber was evacuated using a mechanical rotary vane pump to remove impurities. Ar-3 pct H_2 gas mixture was continuously flushed into the reaction chamber using a mass flow controller at a flow rate of 200 SCCM. Impurities in the Ar-3 pct H_2 gas mixture were removed by passing the gas through Drierite (W.A. Hammond Drierite Co. Ltd., Xenia, OH), silica gel (medium granular material, 5 to 10 mesh), and Mg turnings at 723 K (450 °C).

The experimental temperature was 1823 K (1550 °C), and this was controlled to within ± 2 K (± 2 °C) using a proportional integral differential controller and a B-type (Pt-30 pct Rh/Pt-6 pct Rh) thermocouple covered by an alumina sheath. The experimental time was 1 hour. After stabilization of the experimental temperature, a metal sample (0-minute sample) was initially collected by vacuum suction using a quartz tube (OD: 6 mm; ID: 4 mm), followed by rapid quenching in ice water. Once stabilization of the required temperature was confirmed, industrial EAF slag (60 g) particles of a specific size (~ 2 mm diameter) were quickly added through a quartz tube (OD: 18 mm; ID: 15 mm) to the surface of the molten steel(+ DRI) under an Ar-3 pct H_2 gas mixture atmosphere. After EAF slag addition, metal and slag samples were taken at various time intervals (5, 10, 30, and 60 minutes). Slag samples were collected by dipping the tip of a stainless steel rod into the slag layer only, followed by quenching in ice water. The compositions of materials used in the present study are listed in Table I.

Images were recorded by a camera for specific states of the reaction, *e.g*., melting and slagmaking, and the slag–metal refining reaction. After the experiment was complete, metal samples were polished using a grinder and fine sand paper to remove oxide film on the surface of the samples, and were cut into small pieces of constant weight to reduce analysis error. Fine contaminants remaining on the surface of the metal samples were removed by ultrasonic cleaning. Slag samples were finely crushed using a stainless steel mortar, sieved to under 100 μm, and then formed into beads for chemical analysis using a bead machine (K2, Katanax).

Carbon and sulfur contents in the metal and slag samples were determined using a combustion analyzer (CS-300, LECO). Oxygen content in the metal samples was analyzed using a different type of combustion analyzer (TC-300, LECO). Furthermore, the compositions of metal and slag samples were determined by inductively coupled plasma-atomic emission spectroscopy (ICP-AES, SPECTRO ARCOS, SPECTRO) and X-ray fluorescence spectroscopy (XRF, ZSX PRIMUS IV, Rigaku), respectively. Final steel and slag compositions according to DRI mixing ratio are listed in Table II.

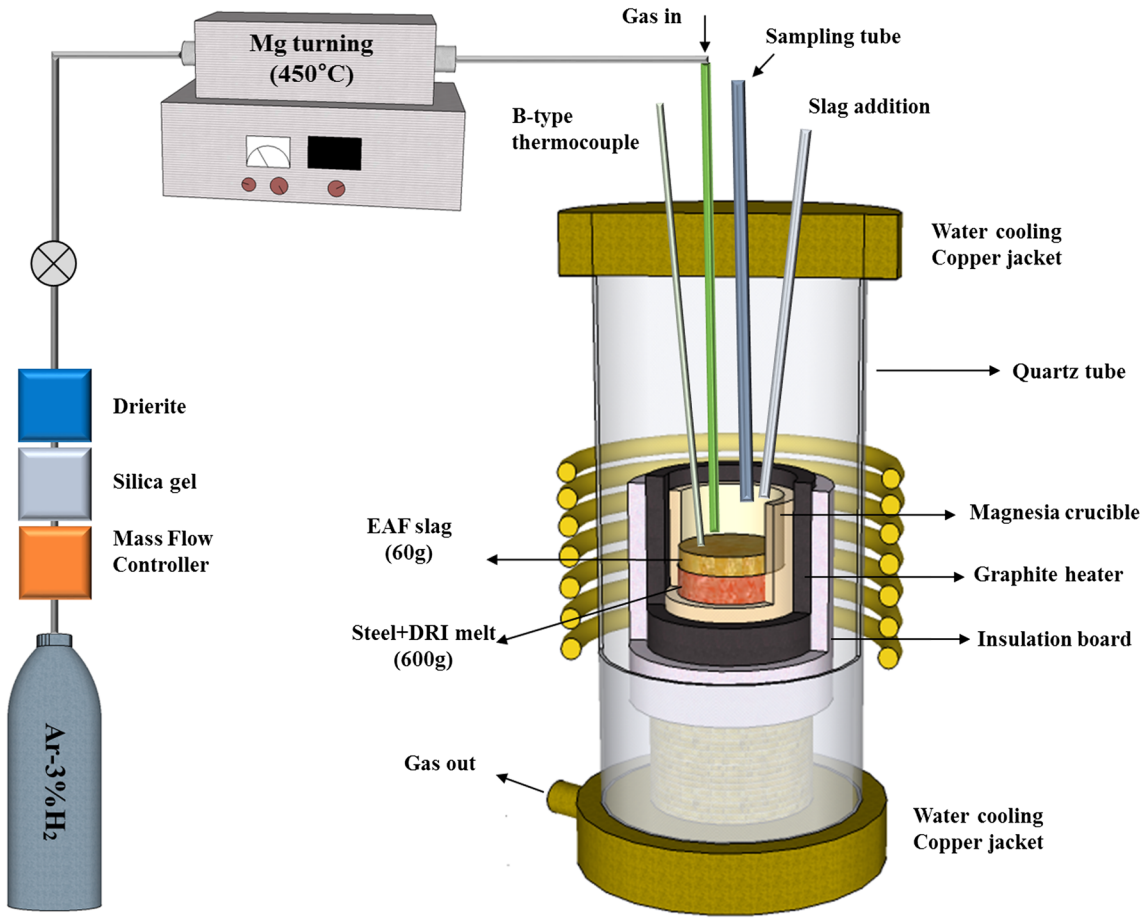

Fig. 1—Schematic diagram of the experimental apparatus.

Table I. Compositions of Materials Used in the Present Study (Mass Pct)

	Fe	Si	Mn	P	S	C	CaO	SiO_2	FeO	Al_2O_3	MgO	MnO	P_2O_5
EAF slag	—	—	—	—	—	—	20.0	16.9	39.6	13.1	3.2	7.2	0.2
DRI	bal.	—	—	0.02	0.02	1.0	1.0	5.0	9.0	—	—	—	—
Steel	bal.	0.03	0.05	0.03	0.03	0.1	—	—	—	—	—	—	—

Table II. Experimental Results

DRI Content (pct)	Steel Composition (Mass Pct)						Slag Composition (Mass Pct)								
	O	C	S	Si	Mn	P	CaO	SiO_2	Al_2O_3	FeO	MgO	MnO	P_2O_5	$\log C_{PO_4^{3-}}$	$\Delta G^{Ex}_{P_2O_5}$
0	0.077	0.015	0.032	0.002	0.031	0.019	21.5	14.0	13.1	37.6	5.9	7.4	0.52	17.3	− 524
10	0.089	0.018	0.028	0.001	0.028	0.019	21.3	15.5	11.3	37.4	7.1	7.0	0.42	17.0	− 510
20	0.106	0.014	0.028	0.002	0.026	0.021	19.1	17.6	11.5	35.8	9.6	6.1	0.32	16.7	− 498
30	0.112	0.007	0.028	0.002	0.030	0.022	18.2	21.7	10.4	34.9	9.5	5.1	0.22	16.4	− 478

III. RESULTS AND DISCUSSION

A. *Reaction Phenomena in Presence of Direct Reduced Iron (DRI)*

It is very important to understand macroscopic reaction phenomena when DRI is used during the slag–metal reaction, and it is also important to study melting behavior when gangue oxides and carbon are present in DRI. Reaction phenomena for the states of initial melting during heating, complete melting, and the slag–metal reaction are shown in Figure 2. Partially melted Fe and CO gas evolution were observed during initial melting, as shown in Figure 2(a). CO gas originated from carbothermic reaction between FeO and carbon in DRI as given in Eq. [1].[27]

$$(FeO) + C(s) = Fe(l) + CO(g), \quad \Delta G^{o}_{[1]} = 141{,}700 - 140T \text{ (J/mol)} \qquad [1]$$

Thereafter, thin slag layer on the surface of molten steel was produced by the melting of gangue oxides in DRI as shown in Figure 2(b) and the absolute quantity of slag produced by gangue oxides in DRI increased with the increasing DRI content. The slag–metal refining reaction and CO gas evolution after addition of EAF slag are shown in Figure 2(c). Slag foaming was induced by CO gas evolution from the reaction between FeO in the molten slag with carbon in the molten steel. At this point, the changes in composition and amount of slag present after EAF slag addition are strongly dependent on DRI content. Therefore, it is vital to evaluate the behavior of phosphorus in molten steel and slag according to DRI mixing ratio during specific reaction stages, such as melting and slag–metal reaction, to thermodynamically understand dephosphorization reaction mechanism.

B. *Effect of DRI Mixing Ratio on Thermodynamic Behavior of Phosphorus in Molten Steel and Slag*

The distribution behavior of phosphorus in steel and slag according to DRI content as a function of reaction time is shown in Figure 3. Two reaction stages—melting, and slag–metal reaction—were examined. As shown in Figure 3(a), even though small amount of slag was formed when DRI was used, phosphorus content in molten steel was not clearly changed during melting stage. This is possibly due to the formation of relatively acidic slag with very small amounts. Thus, dephosphorization capability was not confirmed despite thin slag layer being produced by gangue oxides in DRI (Figure 2(b)).

After confirmation of fully molten state of steel and DRI, further dephosphorization occurred up to about 10 minutes after EAF slag addition except for the case with a 30 pct DRI content. The effect of DRI content on the behavior of phosphorus in molten slag during the slag–metal reaction was clearly confirmed as shown in Figure 3(b). The observed trend in dephosphorization behavior according to DRI mixing ratio can be understood by a change in activity of CaO in molten slag, which will be discussed in Section III-C.

Slag foaming was caused by carbothermic reaction as given in Eq. [1] due to the consumption of carbon in DRI and steel. Carbon and oxygen content in molten steel was therefore expected to differ based on DRI content. Dephosphorization is directly affected by the levels of carbon and oxygen in molten steel. Especially, carbon increases activity coefficient of phosphorus (f_P) in metal phase because the interaction parameter for the effect of carbon on phosphorus in metal phase ($e_P^C = 0.126$ in Table III.[28]) has positive value. This will be discussed further in Section III-C. Therefore, we evaluated the behavior of carbon and oxygen in molten steel as a function of reaction time according to DRI content, as shown in Figure 4.

There were differences in the carbon content at the initial state at different DRI levels (Figure 4(a)). Carbon content in cases with 10, 20, and 30 pct DRI decreased during melting stage because of the carbothermic reaction described in Eq. [1]. No change in carbon content was observed in the case with no DRI. After EAF slag addition, the carbon content in molten steel decreased slightly as a function of reaction time due to reaction of the carbon with FeO in molten slag. Slag foaming due to CO gas evolution (see Figure 2(c)) occurred regardless of whether DRI was present or not.

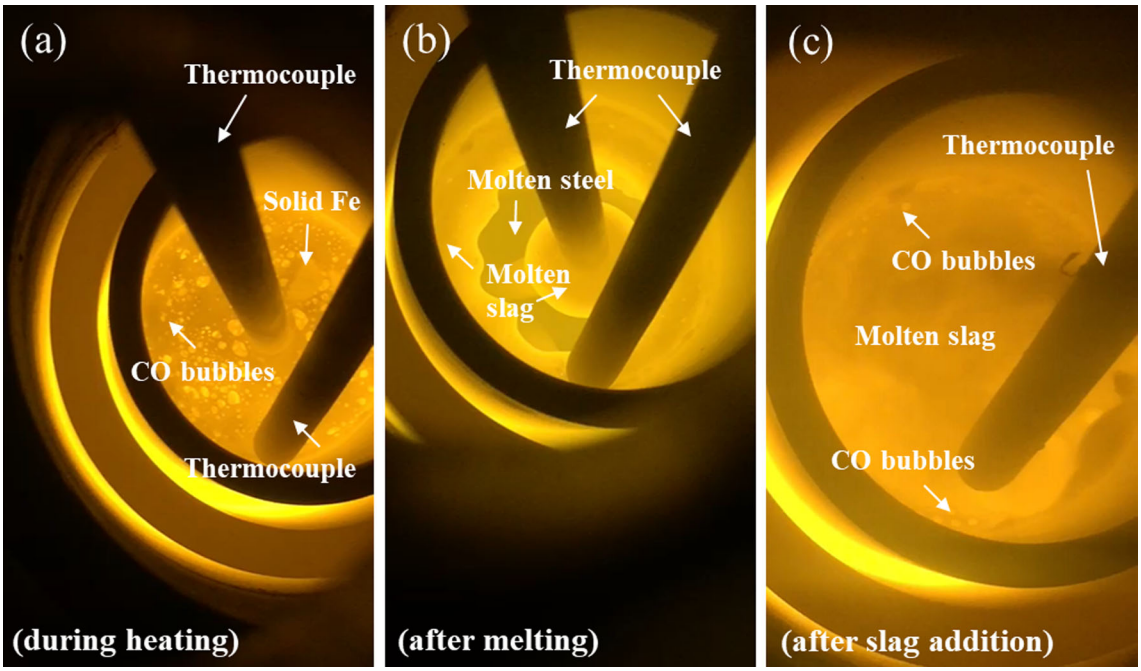

Fig. 2—Snapshot for reaction steps: (*a*) during heating, (*b*) after DRI melting, and (*c*) after slag addition.

The behavior of oxygen in molten steel is shown in Figure 4(b). Oxygen content increased with DRI content during melting stage because the oxygen potential in slag produced by gangue oxides was proportional to the DRI content. After EAF slag addition, oxygen content increased sharply until 10 minutes because of the high oxygen potential of EAF slag. Furthermore, oxygen content increased rapidly to 0.08 to 0.11 mass pct in molten steel regardless of DRI content. Even though the behavior of oxygen showed some fluctuations as a function of reaction time, it was clearly proportional to DRI content. By examining the behavior of phosphorus, carbon, and oxygen at different DRI mixing ratio as a function of reaction time, we confirmed macroscopic reaction phenomena at specific reaction states. However, dephosphorization ability should also be investigated using a thermodynamic approach.

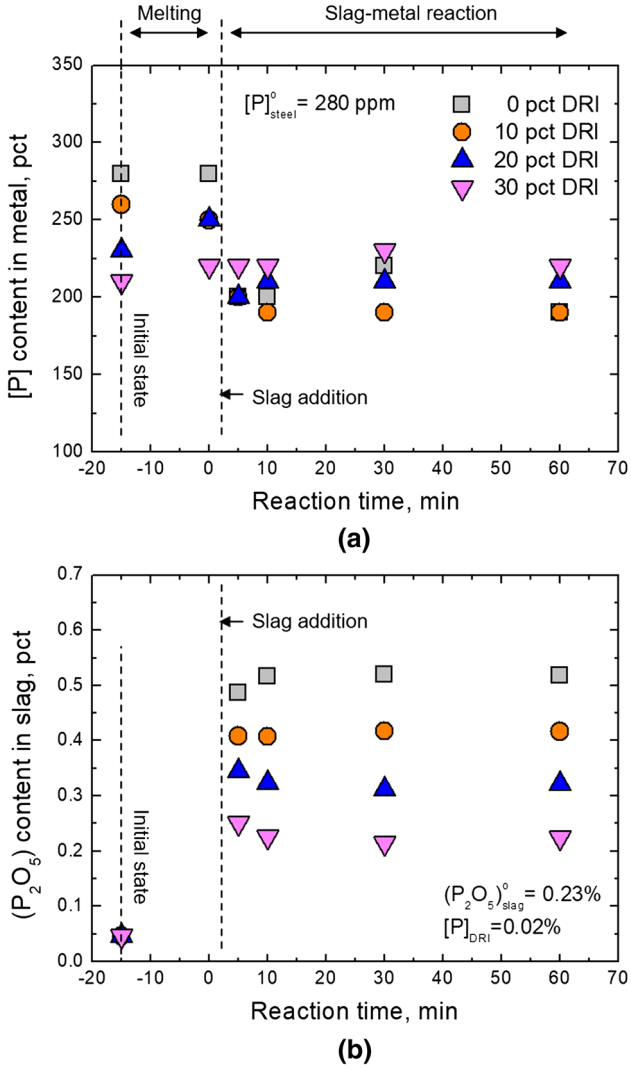

Fig. 3—Contents of (*a*) P in the metal and of (*b*) P_2O_5 in the slag as a function of reaction time at different DRI contents at 1823 K (1550 °C).

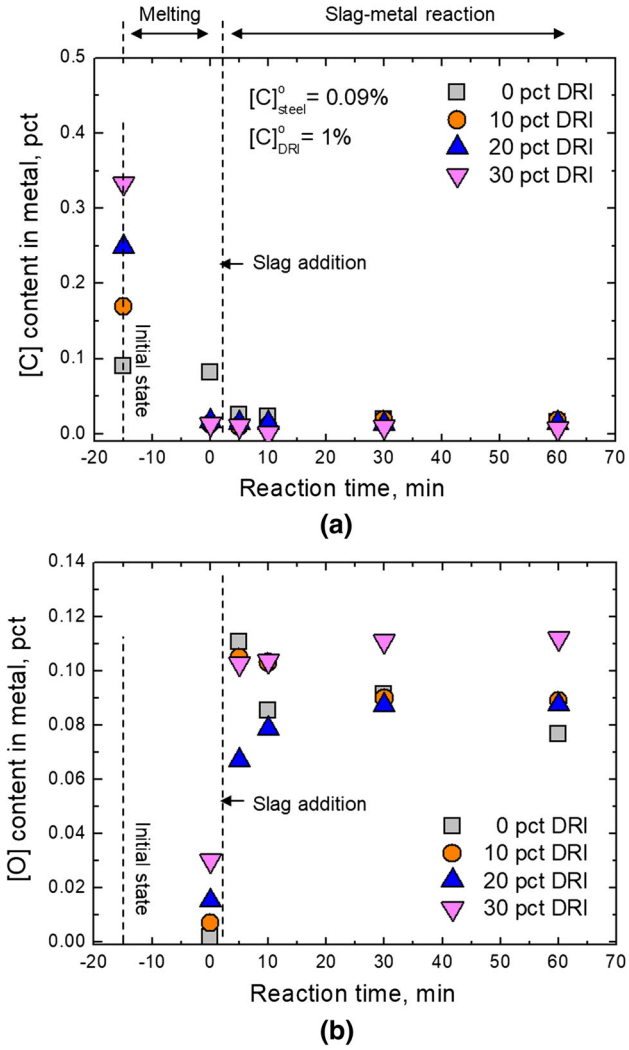

Fig. 4—Contents of (*a*) carbon and (*b*) oxygen in the metal phase as a function of reaction time at different DRI contents at 1823 K (1550 °C).

Table III. Interaction Parameters Used in the Present Study

$e^i_{j=P,O}$	Si	Mn	P	S	C	O
O	− 0.066	− 0.021	0.07	− 0.133	− 0.421	− 0.2*
P	0.099	− 0.032	0.054	0.034	0.126	0.13

*− 1750/T + 0.76.

C. *Effects of DRI Mixing Ratio on Phosphate Capacity and Stability of P_2O_5 in EAF Slag*

Phosphate capacity as a measure of the ability of a slag to absorb phosphorus can be defined as a function of temperature, basicity, and the stability of phosphate ions in the slag as follows[29]:

$$\frac{1}{2}P_2(g) + \frac{3}{2}(O^{2-}) + \frac{5}{4}O_2(g) = (PO_4^{3-}) \quad [2]$$

$$C_{PO_4^{3-}} = \frac{K_{[2]} \cdot a_{O^{2-}}^{3/2}}{f_{PO_4^{3-}}} = \frac{(\text{pct } PO_4^{3-})}{P_{P_2}^{1/2} \cdot P_{O_2}^{5/4}}, \quad [3]$$

where $K_{[2]}$ is the equilibrium constant of Eq. [2], $a_{O^{2-}}$ is the activity of free O^{2-} ions, $f_{PO_4^{3-}}$ is the activity coefficient of phosphate ions in slag, and $P_{i=P_2,O_2}$ is the partial pressure of the gaseous component of *i*. Partial pressures of phosphorus and oxygen can be obtained based on thermodynamic equilibria as follows[30,31]:

$$\frac{1}{2}P_2(g) = \underline{P}\,(\text{mass pct in Fe}), \quad \Delta G^o_{[4]} = -157,700 + 5.4T(\text{J/mol}) \quad [4]$$

$$\frac{1}{2}O_2(g) = \underline{O}\,(\text{mass pct in Fe}), \quad \Delta G^o_{[5]} = -117,200 - 2.9T(\text{J/mol}) \quad [5]$$

Furthermore, the activity coefficients of phosphorus and oxygen in molten steel were calculated from the following equation using the interaction parameters between Si, Mn, P, S, C, and O listed in Table III.[28]

$$\begin{aligned}\log f_{i=O,P} = {} & e_i^{Si}[\text{mass pct Si}] + e_i^{Mn}[\text{mass pct Mn}] \\ & + e_i^{P}[\text{mass pct P}] + e_i^{S}[\text{mass pct S}] \\ & + e_i^{C}[\text{mass pct C}] + e_i^{O}[\text{mass pct O}]\end{aligned} \quad [6]$$

Slag composition is expected to change with DRI content because gangue oxides in DRI dissolve into the slag. In particular, because SiO_2 content in DRI as a gangue oxide is relatively high (*i.e.*, 5 mass pct), slag basicity, which is the driving force of dephosphorization reaction based on Eq. [2], will decrease. Thus, it is vital to confirm the relationship between modified basicity index, *e.g.*, $\log X_{BO(=CaO+Na_2O+BaO+MnO)}/X_{AO(=SiO_2+B_2O_3)}$ and phosphate capacity, $\log C_{PO_4^{3-}}$, as shown in Figure 5.[12–15,23,32] Phosphate capacity, $\log C_{PO_4^{3-}}$, clearly decreased with the decreasing basicity and with the increasing DRI content, indicating that a higher content of DRI unambiguously reduced dephosphorization efficiency by contributing SiO_2.

Im *et al.*[14] studied dephosphorization of carbon-saturated iron by the $CaO\text{-}SiO_2\text{-}Fe_tO$ slag at 1573 K (1300 °C) under $p(O_2) = 10^{-12\sim-14}$ atm. Although slag basicity was relatively low, *viz.* $\log X_{BO}/X_{AO} < 0.2$, $\log C_{PO_4^{3-}}$ was high. Because the dephosphorization reaction is exothermic, the forward reaction proceeds as temperature decreases in Eq. [2]. Moreover, the driving force of dephosphorization is typically proportional to slag basicity. Even though the reaction temperature was relatively high (1873 K [1600 °C]), $\log C_{PO_4^{3-}}$ was high (= 19 to 20) from the results of Nakamura *et al.*[12] This was high for CaO-saturated slag because of its highly basic character. Furthermore, because BaO is more basic than CaO, addition of BaO into the $CaO_{sat}\text{-}SiO_2\text{-}Fe_tO$ slag could further improve phosphate capacity.

Hamano and Tsukihashi [16] also investigated dephosphorization of Fe-0.005 pct P steel by the $CaO_{sat}\text{-}MgO_{sat}\text{-}Fe_tO\text{-}SiO_2\text{-}B_2O_3$ slag at 1873 K (1600 °C) under $p(O_2) = 10^{-10}$ atm. Even though they also used CaO-saturated slag, phosphate capacity, $\log C_{PO_4^{3-}}$, at $\log X_{BO}/X_{AO} < 0.5$ was smaller than that reported by Nakamura *et al.*[12] This is because of the content of B_2O_3 in molten slag (~ 12 mass pct) due to the acidic behavior of B_2O_3 as likely as SiO_2.

Li *et al.*[18] investigated dephosphorization of Fe-1.2 mass pct P steel by the $CaO\text{-}SiO_2\text{-}Fe_tO\text{-}Al_2O_3\text{-}Na_2O\text{-}MgO_{sat}$ slag at 1823 K (1550 °C) and 1873 K (1600 °C) under $p(O_2) = 10^{-10}$ atm, which is a similar slag system to what we investigated in the current study. They reported that addition of a small amount of Na_2O (up to 4 mass pct) to the molten slag increased its phosphate capacity. Even though slag basicity was quite low ($\log X_{BO}/X_{AO} = -0.4$), the $\log C_{PO_4^{3-}}$ value of the $Na_2O\text{-}Fe_tO\text{-}SiO_2\text{-}MgO_{sat}$ slag was similar to the value we obtained due to the high content of Na_2O (5 to 34 mass pct), as described by Sekino and Sano.[23] Furthermore, the $\log C_{PO_4^{3-}}$ value, which was shown to be clearly dependent on the temperature, increased with the decreasing temperature from 1923 K to 1823 K (1650 °C to 1550 °C). However, the $\log C_{PO_4^{3-}}$ value of the $MnO\text{-}SiO_2\text{-}Fe_tO\text{-}MgO_{sat}$ slag was lower than the value we obtained for a similar range of basicity index.[32] Because MnO typically has a lower basic character than CaO, a lower $\log C_{PO_4^{3-}}$ is reasonable. However, the $\log C_{PO_4^{3-}}$ value in the slag shows that it increased with the decreasing temperature from 1923 K to 1673 K

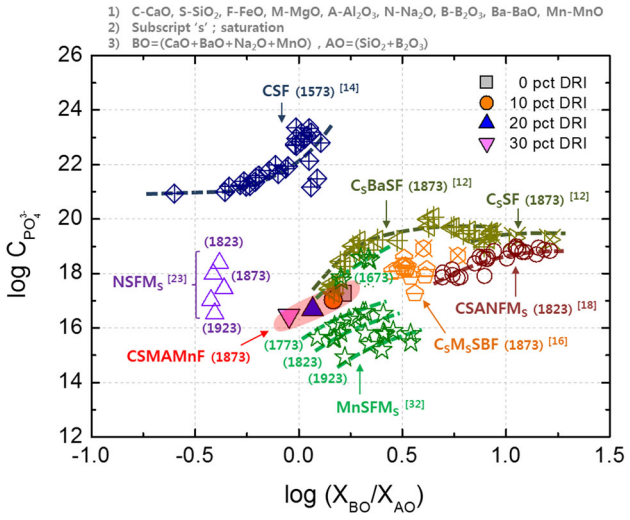

Fig. 5—Phosphate capacity as a function of basicity index, log (X_{BO}/X_{AO}), at different DRI contents.

(1650 °C to 1400 °C). The quantitative understanding of phosphate capacity can be done by evaluating the activity of each slag component.

The iso-activity contours of CaO, SiO_2, and FeO in the $CaO-SiO_2-FeO-10Al_2O_3-5MgO-5MnO$ (mass pct) phase diagram obtained at 1823 K (1550 °C) under $p(O_2) = 10^{-10}$ atm using a commercial thermochemical computing package (FactSage™ 7.0, CRCT Therm-Fact, Inc., Montreal, Canada) are shown in Figure 6. Activity of CaO decreases and that of SiO_2 increases with the increasing DRI content. The activity of FeO remains constant at about 0.6. CaO is known to behave as a representative basic component by contributing free oxygen ions (O^{2-}) in the slag as outlined in the following reactions[33]:

$$(CaO) = (Ca^{2+}) + (O^{2-}) \quad [7]$$

$$a_{O^{2-}} = \frac{K_{[7]} \cdot a_{CaO}}{a_{Ca^{2+}}} \quad [8]$$

By combining Eqs. [3] and [8], the correlation between CaO activity and phosphate capacity can be deduced as follows:

$$\log C_{PO_4^{3-}} = \frac{3}{2}\log a_{CaO} - \frac{3}{2}\log a_{Ca^{2+}} - \log f_{PO_4^{3-}} + \text{Const.} \quad [9]$$

Based on Eq. [9], the phosphate capacity and activity of CaO are expected to exhibit a linear relationship with a slope of 1.5 on a logarithmic scale assuming that the compositional dependencies of $a_{Ca^{2+}}$ and $f_{PO_4^{3-}}$ are not critical at a given temperature. Figure 7 shows the linear relationship between phosphate capacity and the activity of CaO obtained using least square regression. The fitted line had a slope of 2.0; this is slightly larger than the theoretical slope of 1.5, indicating a change in $a_{Ca^{2+}}$ and/or $f_{PO_4^{3-}}$ due to the variation of the activity of CaO. In other words, $a_{Ca^{2+}}$ and/or $f_{PO_4^{3-}}$ would be decreased with the increasing activity of CaO. Nevertheless, the activity of CaO can be used as a useful index representing the basicity of slag based on the linear relationship between phosphate capacity and the activity of CaO. It is noteworthy that the phosphate capacity of slag is strongly affected by the activities of CaO and SiO_2 under the present experimental conditions.

The stability of phosphate ions in slag can be understood by examining the excess free energy of P_2O_5 molecule ($\Delta G^{Ex}_{P_2O_5}$) as described in the following equations[20,34]:

$$P_2(g) + \frac{5}{2}O_2(g) = (P_2O_5), \quad \Delta G^{o}_{[10]} = -1,534,000 + 506.4T \text{ (J/mol)} \quad [10]$$

$$\gamma_{P_2O_5} = \frac{K_{[10]} \cdot P_{P_2} \cdot P_{O_2}^{5/2}}{X_{P_2O_5}} \quad [11]$$

$$\Delta G^{Ex}_{P_2O_5} = RT\ln\gamma_{P_2O_5} \quad [12]$$

The excess free energy of P_2O_5 as a function of SiO_2 content in the slags at 1823 K (1550 °C) is shown in Figure 8. The excess free energy increased with the increasing SiO_2 content, representing that the stability of P_2O_5 decreased in the more acidic slag due to higher SiO_2 content, which resulted from the higher DRI mixing ratio in the present study.

D. *Reaction Steps of Dephosphorization in DRI-containing System*

Various reaction phenomena, such as carbothermic reaction and slagmaking by gangue oxides in DRI, were explored in Section III-A. Slagmaking due to melting of gangue oxides in DRI is important for dephosphorization because SiO_2 as an acidic component in DRI

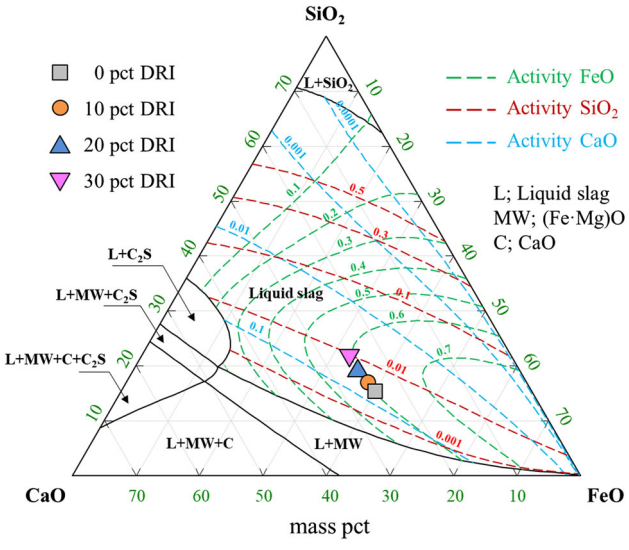

Fig. 6—Iso-activity contours of CaO, SiO_2, and FeO in the $CaO-SiO_2-FeO-10Al_2O_3-5MgO-5MnO$ (mass pct) phase diagram at 1823 K (1550 °C) under $p(O_2) = 10^{-10}$ atm.

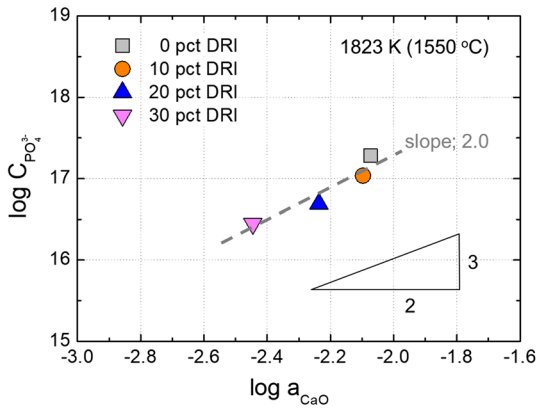

Fig. 7—Relationship between $\log a_{CaO}$ and $\log C_{PO_4^{3-}}$.

decreases the thermodynamic driving force to remove phosphorus, resulting in suppression of dephosphorization efficiency. Thus, the elementary steps of the dephosphorization reaction require elucidation.

We divided the reaction into two stages, namely the melting and reaction (or refining) stages. Steel (represents scrap) and DRI were charged into the furnace crucible (Figure 9(a)) without any chemical reactions. As the temperature was increased, small amounts of slag were formed by melting of gangue oxides present in the DRI (previously shown in Figure 2(a)). CO gas evolution occurred as a result of chemical reaction between FeO and carbon in DRI, but steel as well as DRI remained partially solid. After the experimental temperature (1823 K [1550 °C]) was reached, the steel and DRI were fully melted (previously shown in Figure 2(b)), which we refer to as the melting stage (Figure 9(b)), during which dephosphorization reaction is not occurred due to the relatively acidic characteristics of thin slag layer. In the slag–metal reaction (*i.e.*, refining) stage (Figure 9(c)), a large amount of oxygen dissolved into the molten steel regardless of DRI content because of the high oxygen potential of EAF slag. Furthermore, slag foaming due to CO gas evolution occurred as a result of carbothermic reaction between FeO in molten slag and carbon in steel (previously shown in Figure 2(c)). Degree of dephosphorization was strongly dependent on DRI mixing ratio and thus related to slag basicity. Even though the absolute slag volume in the case with a 30 pct DRI content was greater than that in the case with no DRI, dephosphorization was relatively low in the former because of the lower slag basicity in the case of high mixing ratio of DRI.

In summary, we investigated the effect of DRI mixing ratio on dephosphorization of molten steel *via* EAF slag at 1823 K (1550 °C). Basicity, which is the thermodynamic driving force of dephosphorization reaction, decreased with the increasing DRI mixing ratio because SiO_2 content in the slag increased. The stability of P_2O_5 increased with the decreasing DRI ratio, *i.e.*, SiO_2 content, in terms of the excess free energy of P_2O_5. A

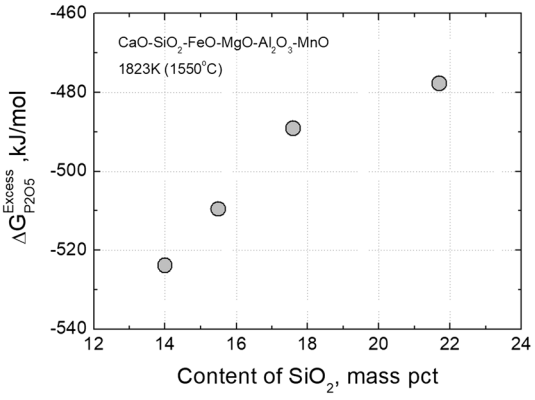

Fig. 8—Excess free energy of P_2O_5 in the slag at 1823 K (1550 °C).

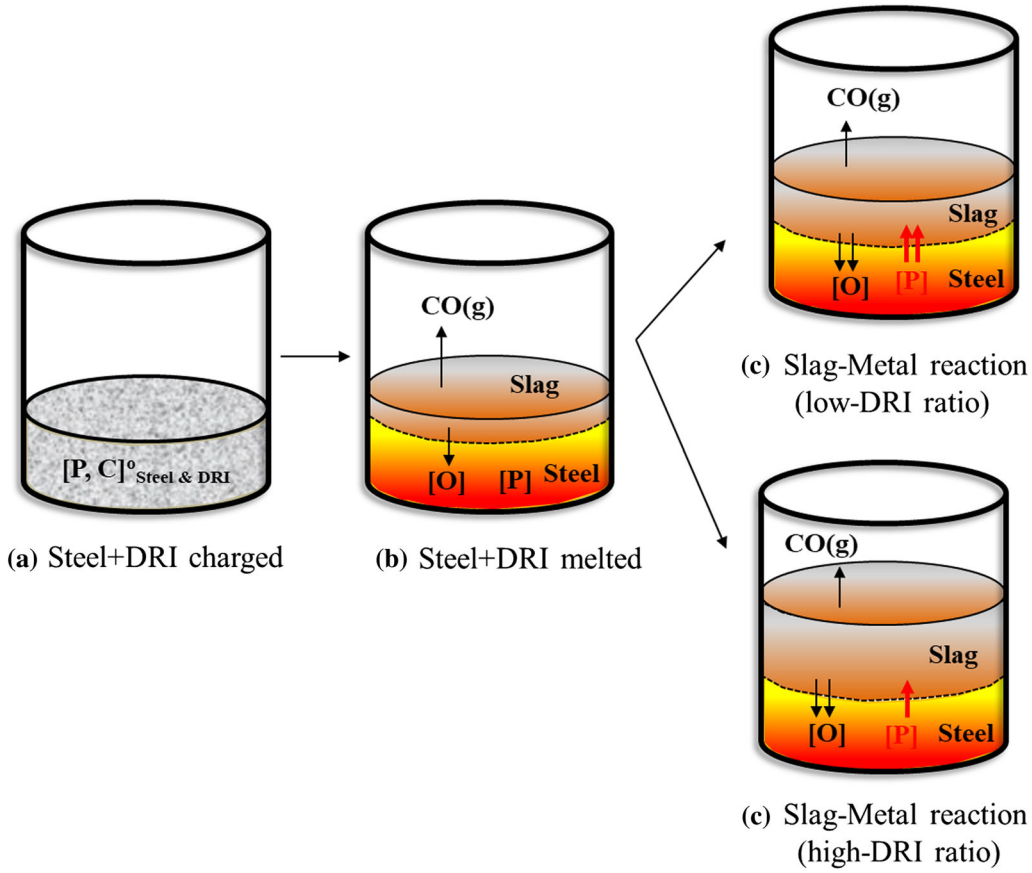

Fig. 9—Schematic reaction steps in the presence of DRI: (*a*) after DRI charging, (*b*) after DRI melting, and (*c*) after slag–metal reaction process.

high content of DRI makes dephosphorization difficult due to its ability to decrease basicity and the stability of P_2O_5 in slag. Therefore, it is very important to increase basicity to improve the dephosphorization efficiency in DRI-used EAF operations.

IV. CONCLUSIONS

We investigated the effect of DRI mixing ratio on the dephosphorization of molten steel *via* EAF slag at 1823 K (1550 °C) and discussed reaction steps of dephosphorization when using DRI. Our major findings can be summarized as follows:

1. Two reaction steps, namely melting and slag–metal reactions (called refining), were experimentally observed. Slagmaking by gangue oxides in DRI and CO gas evolution by carbothermic reaction between FeO and carbon in DRI was observed during heating and melting stages.
2. Behaviors of phosphorus, oxygen, and carbon were evaluated in each reaction step as a function of reaction time, and were clearly dependent on DRI mixing ratio.
3. Basicity, which is the thermodynamic driving force of dephosphorization reaction, decreased with the increasing DRI content because the SiO_2 content in molten slag increased. Furthermore, the stability of P_2O_5 decreased with the increasing DRI content because the slag becomes more acidic.
4. A higher content of DRI made dephosphorization difficult by decreasing the basicity and stability of P_2O_5 in the slag. Therefore, it is very important to increase basicity to improve the dephosphorization capability in DRI-used EAF process.

ACKNOWLEDGMENTS

This study was partly supported by the Korea Institute of Energy Technology Evaluation and Planning (KETEP) and the Ministry of Trade, Industry & Energy (MOTIE) of the Republic of Korea (Grant No. 20172010106310). In addition, this study was partly supported by the Industrial Strategic Technology Development program (Grant No. 10044453).

REFERENCES

1. R.D. Morales, A.N. Conejo, and H.H. Rodriguez: *Metall. Mater. Trans. B*, 2002, vol. 33, pp. 187–99.
2. T. Harada and H. Tanaka: *ISIJ Int.*, 2011, vol. 51, pp. 1301–07.
3. M. Kirschen, K. Badr, and H. Pfeifer: *Energy*, 2011, vol. 36, pp. 6146–55.
4. A.A. Maneti, P. Duarte, and J. Morales: *Proc. AISTech*, 2016, vol. 2016, pp. 64–70.
5. F. Memoli: *Proc. AISTech*, 2016, vol. 2016, pp. 91–100.
6. I. Valdez, G. Wilson, A. Brezinski, M. Clayton, J. Cole S. Gonzalez: *Proc AISTech*, 2017, vol. 2017, pp. 1015–25.
7. R.L. González, F.L. Acosta, M. Lowry, D. Kundrat, A. Wyatt, J. Kuntze, and H. Fuchs: *Proc. AISTech*, 2017, vol. 2017, pp. 1035–41.
8. T.A. Bloom, D.R. Fosnacht, and D.M. Haezebrouck: *Iron Steelmak*, 1990, vol. 17, pp. 35–41.
9. R.J. Fruehan and C.P. Manning, AISI/DOE Technology Roadmap Program, Final Report, Oct. 5, 2001, pp. 1–200.
10. H. Suito, R. Inoue, and M. Takada: *Trans. Iron Steel Inst. Jpn.*, 1981, vol. 21, pp. 250–59.
11. H. Suito and R. Inoue: *Trans. Iron Steel Inst. Jpn.*, 1982, vol. 22, pp. 869–77.
12. S. Nakamura, F. Tsukihashi, and N. Sano: *ISIJ Int.*, 1993, vol. 33, pp. 53–58.
13. O.I. Ostrovski, Y.I. Utochkin, A.V. Pavlov, and R.A. Akberdin: *ISIJ Int.*, 1994, vol. 34, pp. 849–51.
14. J. Im, K. Morita, and N. Sano: *ISIJ Int.*, 1996, vol. 36, pp. 517–21.
15. J. Katsuki, Y. Yashima, T. Yamauchi, and M. Hasegawa: *ISIJ Int.*, 1996, vol. 36, pp. S73–S76.
16. T. Hamano and F. Tsukihashi: *ISIJ Int.*, 2005, vol. 45, pp. 159–65.
17. C.M. Lee and R.J. Fruehan: *Ironmak. Steelmak.*, 2005, vol. 32, pp. 503–08.
18. G. Li, T. Hamano, and F. Tsukihashi: *ISIJ Int.*, 2005, vol. 45, pp. 12–18.
19. S. Basu, A.K. Lahiri, and S. Seetharaman: *Metall. Mater. Trans. B*, 2007, vol. 38B, pp. 357–66.
20. M.K. Cho, J.H. Park, and D.J. Min: *ISIJ Int.*, 2010, vol. 50, pp. 324–26.
21. H. Suito and R. Inoue: *Trans. Iron Steel. Inst. Jpn*, 1984, vol. 24, pp. 47–53.
22. F. Li, X. Li, S. Yang, and Y. Zhang: *Metall. Mater. Trans. B*, 2017, vol. 48B, pp. 2367–78.
23. K. Sekino and N. Sano: *Tetsu-to-Hagane*, 1987, vol. 73, pp. 988–95.
24. J.J. Pak and R.J. Fruehan: *Metall. Mater. Trans. B*, 1991, vol. 22B, pp. 39–46.
25. M. Lee, D. Trotter, and O. Mazzei: *Scand. J. Metall.*, 2001, vol. 30, pp. 286–91.
26. A.I. Hassan, G.I. Kotelnikov, A.E. Semin, and G.M. Megahed: Proc. 24th Int. Conf. on Metall. Mater., (*Metal 2015),* Brno, Czech Republic, 2015.
27. E.T. Turkdogan: *Physical Chemistry of High Temperature Technology*, Academic Press, New York, 1980, pp. 1–24.
28. M. Hino and K. Ito: *Thermodynamic Data for Steelmaking*, The 19th Committee in Steelmaking , The Japan Society for Promotion of Science, Tohoku University Press, Sendai, 2010 , pp. 259–64.
29. C. Wagner: *Metall. Trans. B*, 1975, vol. 6B, pp. 405–09.
30. M. Yamamoto, K. Yamada, L.L. Meshkov, and E. Kato: *Tetsu-to-Hagane*, 1980, vol. 66, pp. 2032–39.
31. T.A. Engh, C.J. Simensen, and O. Wijk: *Principles of Metal Refining*, Oxford University Press, Oxford, 1992.
32. Y. Kobayashi, N. Yoshida, and K. Nagai: *ISIJ Int.*, 2004, vol. 44, pp. 21–26.
33. N. Sano: *Advanced Physical Chemistry for Process Metallurgy*, Academic Press, New York, 1997, pp. 45–51.
34. C.H.P. Lupis: *Chemical Thermodynamics of Materials*, North-Holland, New York, 1983, pp. 155–58.